Aerosol and Air Quality Research, 19: 1920–1936, 2019

ISSN: 1680-8584 print / 2071-1409 online
doi: 10.4209/aaqr.2018.06.0222

Evaluation of Iron-based Oxygen Carrier Supported on Alumina/Titania for Charcoal Combustion through Chemical Looping Process

Hsuan-Chih Wu, Young Ku*

Department of Chemical Engineering, National Taiwan University of Science and Technology, Taipei 10607, Taiwan

ABSTRACT

Hematite supported on alumina or alumina/titania was fabricated to serve as an oxygen carrier in the chemical looping combustion (CLC) of charcoal. The reduction rate of Fe_2O_3/Al_2O_3 and $Fe_2O_3/Al_2O_3/TiO_2$ particles increased with the reactor inlet's CO concentration and displayed a slight effect from elevated operating temperatures. Applying the shrinking core model, the mass transfer coefficients (k_g) for the reduction of Fe_2O_3/Al_2O_3 and $Fe_2O_3/Al_2O_3/TiO_2$ by CO were found to be 0.16 and 0.22 mm s^{-1}, respectively, and using the Fe_2O_3/Al_2O_3 and $Fe_2O_3/Al_2O_3/TiO_2$ to combust charcoal resulted in carbon conversion rates of approximately 61.8% and 47.2%, respectively, when the inlet steam flow rate was set to 221.4 mmol min^{-1}. Significantly, a higher inlet steam flow rate may not be advantageous when employing iron-based oxygen carriers. More heat was released during combustion with the Fe_2O_3/Al_2O_3 than with the $Fe_2O_3/Al_2O_3/TiO_2$ due to a high flow rate for the former being used. When $Fe_2O_3/Al_2O_3/TiO_2$ was used as the oxygen carrier, the particles, which contained a large percentage of Fe_2O_3, exhibited high reactivity to syngas (CO/H_2); thus, less $Fe_2O_3/Al_2O_3/TiO_2$ than Fe_2O_3/Al_2O_3 was required to combust the charcoal.

Keywords: Chemical looping process; Charcoal combustion; Hematite; Reduction kinetic; Moving bed reactor.

INTRODUCTION

Coal is the second most important energy source and distributed in many countries (WEC, 2016). Based on the Monthly Energy Review reported by the U.S. Energy Information Administration (EIA), coal contributes about 30% to electricity net generation (EIA, 2017). CO_2 is a major category of greenhouse gases (GHGs) generated from traditional thermal power plants and needs reducing emission to mitigate global warming. In the past few decades, the chemical looping process (CLP) has been recognized as an innovative substitute technology for fuel conversion to implement the efficient generation of energy and the inherent separation of CO_2. For chemical looping combustion (CLC) operation, the metal oxides are wrought as the oxygen source to react with fuel, as described by Eq. (1). Subsequently, the reduced particles are oxidized by air for cyclic applications, as described by Eq. (2).

$$C_nH_{2m} + (2n + m)Me_xO_y \rightarrow nCO_2 + mH_2O + (2n + m)Me_xO_{y-1} \quad (1)$$

$$2Me_xO_{y-1} + O_{2(g)} \leftrightarrow 2Me_xO_y \quad (2)$$

The Ellingham diagram illustrates the variation of oxidation Gibbs free energy (ΔG) with temperature for various compounds. Metal oxides in the Ellingham diagram, such as CuO, NiO, Fe_2O_3, Mn_2O_3, CoO, and $CaSO_4$, have strong oxidizing properties and can work as oxygen carriers for both full oxidation and partial oxidation (Fan *et al.*, 2015; Luo *et al.*, 2015). Zhou *et al.* (2014) studied the CLC of methane in a fixed bed reactor and a fluidized bed reactor using nickel oxide as the oxygen carrier and reported that the CO_2 selectivity and fuel conversion of methane combustion reached above 95%. Cao *et al.* (2014) demonstrated high reactivity for CuO/Al_2O_3 oxygen carrier reduction with H_2, and also reported that the oxygen releasing performance and thermal stability of the copper-based oxygen carrier were significantly impacted by the supporting material (Al_2O_3). The reaction mechanisms and kinetic parameters were determined by Wang *et al.* (2016) using Mn-based oxygen carriers for oxygen release in a fixed bed reactor. Compared to other materials, high melting point, high mechanical strength, and low cost are major advantages have been reported for an iron-based oxygen carrier (Chiu and Ku, 2012). Hence, hematite (Fe_2O_3) is considered to be a reliable and appropriate oxygen carrier for CLC implementation (Luo *et al.*, 2014a; Mattisson *et al.*, 2004). In order to retard agglomeration and attrition of the oxygen carrier, coupling

* Corresponding author.
Tel.: +886-2-2378-5535; Fax: +886-2-2737-6644
E-mail address: ku508@mail.ntust.edu.tw

of hematite with support materials, such as $MgAl_2O_4$, SiO_2, ZrO_2, MgO, Al_2O_3 and TiO_2, can improve the thermal and mechanical stability of oxygen carriers for CLC operation (Abad *et al.*, 2007; Leion *et al.*, 2008; Adánez *et al.*, 2010; Chiu *et al.*, 2014a; Ku *et al.*, 2014). Ismail *et al.* (2014) and Sun *et al.* (2017) found that the addition of CaO and CeO_2 can promote the reactivity of iron-based oxygen carrier reaction with gaseous fuel. Zafar *et al.* (2006) found that the $Fe_2O_3/MgAl_2O_4$ oxygen carrier showed high reactivity with methane, whereas the SiO_2-supported Fe_2O_3 may not be feasible oxygen carrier due to the unreactive iron silicate was formed at high temperature. Dharanipragada *et al.* (2017) indicated that the activation energies of $Fe_2O_3/MgAl_2O_4$ reaction with H_2 for reaction and diffusion were 104 ± 2.3 and 38 ± 5 kJ mol^{-1}, respectively. Qin *et al.* (2013) reported that the energy barriers of Fe_2O_3, Fe_2O_3/Al_2O_3, Fe_2O_3/MgO and Fe_2O_3/ZrO_2 reduction with CO in the fuel reactor (corresponding to Fe_2O_3 to FeO) was calculated as 2.59, 0.99, 0.98 and 0.83, respectively, while the energy barriers of reduced Fe_2O_3, Fe_2O_3/Al_2O_3, Fe_2O_3/MgO and Fe_2O_3/ZrO_2 oxidization with O_2 in the air reactor was determined to be 0.08, 0.79, 0.2 and 1.14, respectively. The addition of support materials decreased the energy barriers in the reduction period, whereas the energy barriers in the oxidization period are increased. Moghtaderi and Song (2010) and Monazam *et al.* (2013) evaluated the activation energies of 25 kJ mol^{-1} and 50.2–64.8 kJ mol^{-1} for Fe_2O_3/Al_2O_3 and Fe_2O_3/MgO reduction with methane. Li *et al.* (2011) indicated the O^{2-} diffusivity of iron-based oxygen carrier was enhanced by using TiO_2 as support because of the lower energy barrier for O^{2-} migration within the dense solid phase. In comparison with the above support materials, Al_2O_3 and TiO_2 are a promising support material due to its high mechanical resistance, proper chemical and physical stability, and high melting point, and frequently applied to improve the thermal and mechanical stability of oxygen carriers for CLC operation. Chiu *et al.* (2014a) characterized the reduction mechanism of Fe_2O_3/Al_2O_3 oxygen carrier and observed high CO_2 yields for syngas and methane combustion in a fixed bed reactor. Liu *et al.* (2016) indicated that Fe_2O_3/TiO_2 oxygen carriers containing 20–30 wt.% TiO_2 sintered at 1100°C delivered high CO_2 concentration and H_2 conversion. However, the disintegration of Fe_2O_3/TiO_2 oxygen carrier structure was caused by the interaction between metallic Fe and reduced TiO_{2-x} or titania species occurred during the redox cycle operation. Ku *et al.* (2017) proposed the iron cations' diffusion mechanism of Fe_2O_3/Al_2O_3 and Fe_2O_3/TiO_2 pellets during reduction and oxidation operations and also indicated that the Fe_2O_3/TiO_2 pellets exhibited approximately 2 times more attrition loss than Fe_2O_3/Al_2O_3 pellets. Kuo *et al.* (2015) found that the $NiFeAlO_4$ oxygen carrier provided high CO conversion and H_2 generation. Recently, more complex materials are developed and studied for chemical looping process, including perovskite-type oxides, spinel-type oxides, and mixed-metal oxides (Ksepko *et al.*, 2016). Nevertheless, most of the studies were limited to mono-support oxygen carrier. Co-support oxygen carrier has not been extensively applied for the chemical looping process. Therefore, in this study, Fe_2O_3 supported on Al_2O_3-TiO_2 co-support was prepared and used in evaluating its feasibility to be an oxygen carrier for CLC application.

The classification of coal can be divided into four categories, including anthracite, bituminous coal, sub-bituminous coal and lignite (brown coal) (IEA, 2009). Several researches have been performed in the continuous CLC facilities for coal as feedstock (Berguerand and Lyngfelt, 2008; Sozinho *et al.*, 2012; Gu *et al.*, 2014; Mendiara *et al.*, 2014; Ströhle *et al.*, 2015). Song *et al.* (2012) utilized the Shenhua coal and Xuzhou coal as solid fuels to evaluate the effect of char gasification efficiency on the CLC with hematite ore in a 1 kW_{th} fluidized bed reactor, and also reported that CO_2 concentration at the fuel reactor outlet was increased with increasing char gasification efficiency, further validating that char gasification products react fast with the hematite ore. Markström *et al.* (2013) presented the design and operation of CLC with Colombian coal in a 100 kW_{th} fluidized bed reactor with ilmenite and indicated that the highest gas conversion and CO_2 capture efficiency of coal combustion reached about 84.1% and 96.4–99.5% for experiments conducted at 940–980°C in the fuel reactor, respectively. Furthermore, Linderholm and Schmitz (2016) reported that the highest gas conversion of nearly 87% was achieved for both Colombian coal and Calenturitas coal combustion with hematite ore, while the CO_2 capture efficiencies were obtained to be 94–98%.

Thon *et al.* (2014) applied a 25 kW_{th} two-stage fluidized bed reactor to investigate the CLC of lignite dust with Australian ilmenite and greater than 90 vol.% of CO_2 concentration could be achieved at the fuel reactor outlet. However, the reason is needed to be further investigated for the unconverted combustible gases appeared in the fuel reactor exhaust gas. Bayham *et al.* (2013) indicated that the carbon conversions were confirmed more than 90% for the combustion of both sub-bituminous coal and lignite coal using a 25 kW_{th} moving bed reactor operated with iron-based oxygen carriers, while CO_2 concentration in the fuel reactor outlet stream was obtained to be 99.5 vol.%. Kim *et al.* (2013) reported that carbon conversion for sub-bituminous coal and metallurgical coke combustion were found to be 97% and 81%. The carbon conversion for metallurgical coke combustion was lower than that for sub-bituminous coal combustion due to the reactivity of metallurgical coke was less than sub-bituminous coal. Hence, longer residence time was required for complete conversion of metallurgical coke. In addition, high CO_2 purity (> 99%) was obtained for both solid fuel combustion, further indicating that the counter-current moving-bed configuration for the fuel reactor is more effective in fully converting fuels to CO_2 and H_2O as compared to the fluidized-bed system. Biomass is considered to be a promising alternative resource for partial replacement of coal to generate sustainable energy in the future. In recent years, several biomasses have been developed and applied for chemical looping technology (Shen *et al.*, 2009; Gu *et al.*, 2011; Mendiara *et al.*, 2013). Charcoal is a promising solid fuel due to its lower moisture content, higher calorific value,

lower tendency to biodegradation, and easy to pulverize like coal (Gucho *et al.*, 2015; Strandberg *et al.*, 2015). Wu and Ku (2016) indicated that the maximum fuel conversion and oxygen carrier conversion for chemical looping gasification (CLG) of charcoal with Fe_2O_3/Al_2O_3 oxygen carrier were found to be 11.5% and 38.3%, respectively, and also reported that more syngas (CO/H_2) were generated for charcoal gasification conducted in the moving bed reactor operated with higher oxygen carrier-to-fuel ratios.

In this study, alumina/titania-supported Fe_2O_3 oxygen carrier was fabricated to investigate its reactivity with CO by comparing to the Al_2O_3 supported Fe_2O_3 oxygen carrier. In order to understand the kinetics of the reduction with CO, the influences of various experimental parameters on the reduction rate of Fe_2O_3/Al_2O_3 or $Fe_2O_3/Al_2O_3/TiO_2$ oxygen carriers in a fixed bed reactor were discussed and expressed using a shrinking core model (SCM). Furthermore, the present study was also aimed at applying the chemical looping process using the Fe_2O_3/Al_2O_3 and $Fe_2O_3/Al_2O_3/TiO_2$ oxygen carriers to combust charcoal. Carbon conversion and oxygen carrier conversion were determined from the gaseous composition at the moving bed reactor exhaust. The crystalline phases of the reduced oxygen carrier were identified for the samples drawn out from the reactor.

EXPERIMENTAL

Oxygen Carriers

Hematite (99.9% Fe_2O_3; China Steel Corp.) particles were dispersed in deionized water as Fe_2O_3 slurry. Alumina (99% Al_2O_3; Chin Jung Trading Co.), utilized as a support material, was added into the Fe_2O_3 slurry solution to enhance the mechanical strength of Fe_2O_3/Al_2O_3 particles. The mixed solution was stirred vigorously for 10 min and dried at 130°C. The cakes were then pulverized and screened their particle sizes from 1.2 to 1.4 mm. Finally, the particles were calcined in air at 1300°C for 2 h. For the preparation of $Fe_2O_3/Al_2O_3/TiO_2$ particles, a predetermined amount of titania (95.5% TiO_2; Unique Enterprise Co.) was added into the slurry solution containing Fe_2O_3 and Al_2O_3. The $Fe_2O_3/Al_2O_3/TiO_2$ particle was thereafter fabricated by mechanical mixing described in the above section. The prepared $Fe_2O_3/Al_2O_3/TiO_2$ particles were then put in a muffle furnace and calcined isothermally at 1200°C for 2 h. The weight percentage for Fe_2O_3/Al_2O_3 and $Fe_2O_3/Al_2O_3/TiO_2$ particles were determined to be 60/40 and 70/20/10. Crush strength and attrition of prepared particles were measured by a texture machine (TA.XTPlus) and an attrition analyzer following ASTM methods D4058-96. The true density, particle density and bulk density of prepared oxygen carriers were determined by Eqs. (3) and (4), respectively, similar defines and results were reported by previous researchers (Markström and Lyngfelt, 2012):

$$\rho_p = (1 - \varphi)\rho_t \tag{3}$$

$$\rho_b = (1 - \varepsilon)\rho_p \tag{4}$$

where ρ_t is the true density of the oxygen carrier without the pores which presented in the oxygen carrier; ρ_p is the particle density of the oxygen carrier including the pores, which was measured by the Archimedes method; ρ_b is the bulk density of the oxygen carrier; φ is 49.13% and 59.60% as the porosity of prepared Fe_2O_3/Al_2O_3 and $Fe_2O_3/Al_2O_3/TiO_2$, respectively; ε is the fraction of void contained in the packed Fe_2O_3/Al_2O_3 and $Fe_2O_3/Al_2O_3/TiO_2$ oxygen carriers, which were determined to be 41.61% and 40.17%, respectively. The main physicochemical properties of both oxygen carriers are shown in Table 1. Firck *et al.* (2016) and Ku *et al.* (2017) illustrated that the crushing strength of oxygen carriers is enhanced with increasing calcination temperature, hence, less crushing strength of $Fe_2O_3/Al_2O_3/TiO_2$ oxygen carriers are obtained may be ascribed to the $Fe_2O_3/Al_2O_3/TiO_2$ oxygen carriers calcined at the lower calcination temperature. Breault *et al.* (2016) indicated that the specific surface area becomes smaller, while the grain size and porosity become larger because the growth of larger grain promoted by high calcination temperature. The physical properties of the iron-based oxygen carriers reported by previous studies were similar to the results of this study that the specific surface areas were obtained to be in the range of 9.06 $cm^2\ s^{-1}$ to 18 $m^2\ s^{-1}$ (Gao *et al.*, 2016; Huang *et al.*, 2016; Ksepko *et al.*, 2017). Huang *et al.* (2016) indicated that the decline of iron-based oxygen carrier reactivity is generally major caused by the specific surface area of oxygen carrier is decreased. However, the satisfactory reactivity of iron ore is observed for experiments carried out with low specific surface areas of particles. The reason is due to the release of lattice oxygen in the oxygen carrier was suggested to be a

Table 1. Main physicochemical properties of the iron-based oxygen carriers.

Parameters	Unit	Fe_2O_3/Al_2O_3	$Fe_2O_3/Al_2O_3/TiO_2$
Fe_2O_3 fraction	wt.%	60	70
Particle size	mm	1.2–1.4	1.2–1.4
True density, ρ_t	kg m^{-3}	4673	4795
Particle density, ρ_p	kg m^{-3}	2377	1937
Bulk density, ρ_b	kg m^{-3}	1388	1159
Porosity	%	49.13	59.60
Fraction void	%	41.61	40.17
Crushing strength	N	30.53	10.25
Attrition	%	4.01	16.83
Specific surface area, BET	$m^2\ g^{-1}$	0.61	0.64

nucleation and nuclei growth process, thus the reactivity of oxygen carrier is not individually influenced by the surface structure of the particles (Huang *et al.*, 2016). Additionally, Ksepko *et al.* (2017) illustrated that the reactivity and oxygen transfer capacity of the calcined Sinai ore cannot be ascribed only to the small surface area of particles, while the bulk diffusion is considered to be contributed to the reaction kinetics. As mentioned above, the surface area is a key governing factor for evaluating the basic properties of the oxygen carrier, which also may influence the reaction kinetics of the oxygen carrier with fuel gas.

Solid Fuel

Charcoal was applied as the solid fuel for studying the reaction behavior of solid fuels with oxygen carrier in a moving bed reactor. The commercial grade charcoal used in this study was purchased from Puguang Co., Ltd. and all experimental charcoal particles were pulverized and sieved for size between 1.2 mm and 1.4 mm. Thermogravimetric analyzer (TGA; STA 449 F3 Jupiter; Netzsch) was utilized to investigate the proximate analysis of charcoal up to 700°C with a heating rate of 20°C min^{-1}. The elemental analyzer (vario EL III; Elementar) was used to identify the elemental contents of C, H, O, N, and S. The fuel characteristics of the charcoal obtained based on the experimental results are listed in Table 2.

Fixed Bed Reactor System

Experiments were carried out in a cylindrical stainless steel 310S column of 200 mm height and 25.4 mm inner diameter, which was kept isothermal at the desired temperature, ranging from 875 to 925°C. A porous plate was installed inside the reactor to support the predetermined amount of prepared Fe_2O_3/Al_2O_3 or $Fe_2O_3/Al_2O_3/TiO_2$ particles. For reduction experiments, carbon monoxide was introducing into the reactor at a flowrate of 1 L min^{-1} at different concentrations, ranging from 5 to 20%. After reduction, the nitrogen gas flowed to the reactor until the concentration of reducing gas in the reactor was removed. The reduced particles were subsequently oxidized for 30 min at an air flow rate of 1 L min^{-1}. The discharged streams were sampled at predetermined time intervals and measuring the concentration of gaseous product by a non-dispersive infrared sensor (NDIR; Model 6000i Series; Molecular Analysis).

Moving Bed Reactor System

Fig. 1 shows the reaction system employed in this research contained an annular dual-tube moving bed reactor (ADMBR) made entirely of stainless steel 310S (outlet diameter: 76.20 mm) as depicted in our previous research (Wu *et al.*, 2015). The operating temperature of the reactor was maintained at 850–900°C by a PID-controlled electric heating element. The flow rate of charcoal throughout the experiment was kept at 1.05 g min^{-1}. Steam molar flow rates were maintained constant at the desired rate with the N_2 flow rate of 2.2 L min^{-1}. Before starting the CLC experiments, the ADMBR was filled with the Fe_2O_3/Al_2O_3 particles (3.0 kg) or $Fe_2O_3/Al_2O_3/TiO_2$ particles (2.5 kg) of a known amount. Subsequently, the Fe_2O_3/Al_2O_3 and $Fe_2O_3/Al_2O_3/TiO_2$ feeding rate were fixed at 21.79 g min^{-1} and 7.55 g min^{-1}, respectively. For experiments conducted under different conditions, samples of gaseous products were collected at predetermined time intervals from the ADMBR. The screw conveyor was used to draw out the solid samples and residues from the bottom of the ADMBR. All of the solid products were then oxidized at 600°C for 12 h in a muffle furnace. Here, the oxygen carrier particles were separated manually from the ash. A CLC system usually consists of a fuel reactor, an air reactor, and a cyclone. In the whole CLC system, smaller ash is relatively easier to be separated from the reactor through the cyclone. An NDIR sensor (Model 6000i Series; Molecular Analysis) was used for analyzing the gaseous product concentrations in the discharged streams. The concentrations of hydrogen in the effluent streams were determined with a China Chromatography Model 2000 gas chromatograph (GC) equipped with a thermal conductivity detector.

RESULTS AND DISCUSSION

Kinetic Parameter Determination

The mechanisms of gaseous and solid fuel combustion with oxygen carrier have been proposed by previous studies (Adánez *et al.*, 2012; Chiu and Ku, 2012) and are illustrated in Fig. 2. Gaseous fuel can directly react with the oxygen carrier to form CO_2 and H_2O, while the chemical reaction of solid fuel with an oxygen carrier takes place in two steps. The combustible gases generated during the solid fuel gasification, and then oxygen carrier was reduced by the gasified syngas (CO/H_2). Hence, the kinetic study of solid fuel gasification and oxygen carrier reduction should be simultaneously considered for CLC of solid fuel in order to preliminarily assess the performance of the prepared oxygen carrier for solid fuel combustion. In this study, carbon monoxide (CO) used as reducing gas to determine the reduction kinetic parameters of Fe-based oxygen carriers.

The iron-based oxygen carriers were fully reduced for carbon monoxide combustion as described by Eq. (5) (Fan, 2010):

$$CO + \frac{1}{3}Fe_2O_3 \leftrightarrow \frac{2}{3}Fe + CO_2 \quad (5)$$

Table 2. Proximate and ultimate analysis of charcoal.

Fuel	Proximate analysis (wt.%)				Ultimate analysis (wt.%)					HHV
	M	VM	FC	AW	N	C	H	O	S	(MJ kg^{-1})
Charcoal	1.18	0.55	90.79	2.48	0.88	83.41	2.11	2.69	0.08	31.32

M: Moisture; VM: Volatile Material; FC: Fixed Carbon; A: Ash; HHV: Higher Heating Value.

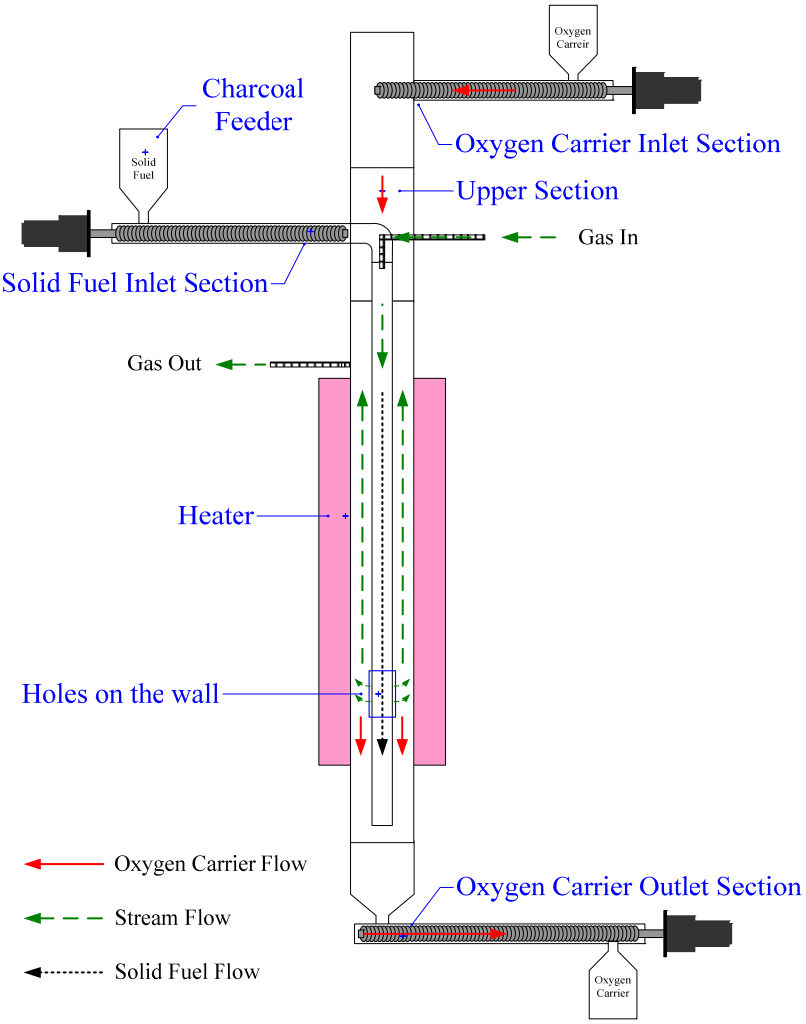

Fig. 1. Moving bed reactor system experimental setup.

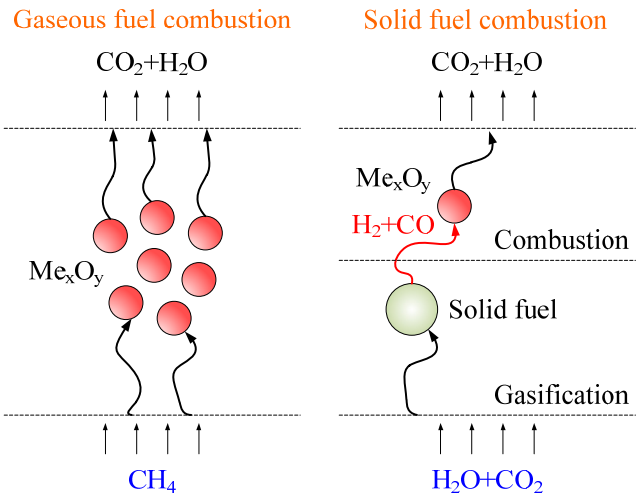

Fig. 2. Reaction mechanisms for gaseous and solid fuel combustion with oxygen carrier by CLC.

Based on the mass balances of oxygen and carbon, the reduction conversion of iron-based oxygen carriers for carbon monoxide combustion is determined as:

$$X_{red} = \frac{\int \left(F_{CO_2} + F_{CO} - F_{CO,in} \right) dt}{\left(\frac{x_{Fe_2O_3} \cdot m_{OC}}{M_{Fe_2O_3}} \right)} \quad (6)$$

where $F_{CO,in}$ denotes the initial flow rate (mmol min^{-1}) of CO; F_{CO} and F_{CO_2} are the flowrate (mmol min^{-1}) of CO and CO_2 in the effluent stream after time t; $M_{Fe_2O_3}$ denotes the molar mass of Fe_2O_3; m_{OC} denotes the packing weight (g) of iron-based particles; $x_{Fe_2O_3}$ denotes the Fe_2O_3 content of the iron-based particles. Fig. 3 shows the effect of operating temperature on the reduction of iron-based oxygen carriers with CO. The reduction conversions of Fe_2O_3/Al_2O_3 oxygen carriers for CO combustion were increased with operation time and were slightly influenced with increasing operating temperatures. However, X_{red} for CLC of CO with $Fe_2O_3/Al_2O_3/TiO_2$ particles was enhanced for experiments conducted with longer operation time, and gradually maintained to about 33%, while reduction of $Fe_2O_3/Al_2O_3/TiO_2$ particles was similar for experiments carried out at operating temperature ranged from 875 to 925°C. Fig. 4 exhibits the effect of inlet carbon monoxide

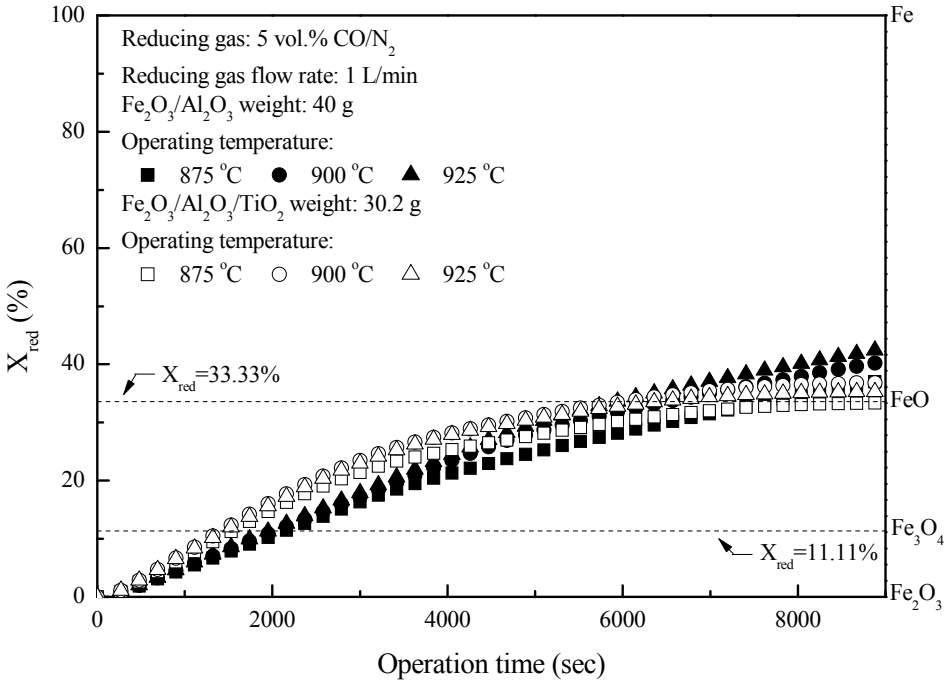

Fig. 3. Effect of operating temperature on the reduction of Fe_2O_3/Al_2O_3 and $Fe_2O_3/Al_2O_3/TiO_2$ with CO in the fixed bed.

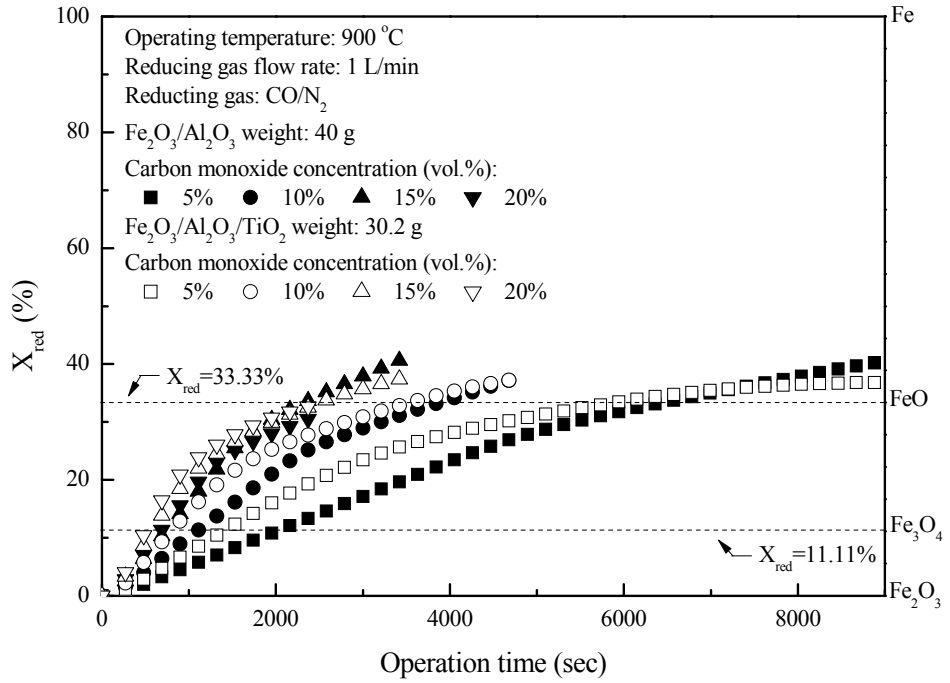

Fig. 4. Effect of inlet CO concentrations on the reduction of Fe_2O_3/Al_2O_3 and $Fe_2O_3/Al_2O_3/TiO_2$ with CO in the fixed bed.

concentrations on the CLC of CO by iron-based oxygen carriers. The conversions of Fe_2O_3/Al_2O_3 and $Fe_2O_3/Al_2O_3/TiO_2$ reduction were increased for experiments conducted with greater inlet CO concentrations, possibly because of the existence of more carbon monoxide molecules. More carbon monoxide molecules are more ready to react with Fe_2O_3 contained in the iron-based oxygen carriers to create carbon dioxide.

In this study, the temporal reduction behavior of iron-based oxygen carrier was described by a shrinking core model (SCM). The similar applications were exercised in the previous researches (Abad *et al.*, 2007; Cabello *et al.*, 2014; Abad *et al.*, 2015).

$$1 - X_{red} = \left(\frac{r}{R}\right)^3 \tag{7}$$

$$t = \tau_{gf} X_{red} + \tau_{pl}\left[1-3\left(1-X_{red}\right)^{\frac{2}{3}}+2\left(1-X_{red}\right)\right] \quad (8)$$

$$\tau_{gf} = \frac{1000 \cdot x_{Fe_2O_3} \cdot \rho_P \cdot R}{3 \cdot b \cdot C_{Ag} \cdot M_{Fe_2O_3} \cdot k_g} \quad (9)$$

$$\tau_{pl} = \frac{1000 \cdot x_{Fe_2O_3} \cdot \rho_P \cdot R^2}{6 \cdot b \cdot C_{Ag} \cdot M_{Fe_2O_3} \cdot D_e} \quad (10)$$

$$D_e = D_{pl,0} \cdot e^{-\frac{Ea_{pl}}{R_g T} - k_d X_{red}} \quad (11)$$

$$k_d = k_{d,0} \cdot e^{-\frac{Ea_d}{R_g T}} \quad (12)$$

where R and r are the radius (m) of the fresh particle and the unreacted core; τ_{gf} and τ_{pl} are the time (s) required for complete conversion of the oxygen carrier when the reaction is controlled by the gas-film diffusion and the product layer diffusion; C_{Ag} is the inlet molar concentration (mol m^{-3}) of the gaseous fuel; b denotes the stoichiometric coefficient, which is determined to be 1/3 by Eq. (5); k_g denotes the mass transfer coefficient (m s^{-1}) between gaseous fuel and oxygen carriers; D_e denotes the effective diffusion coefficient (m^2 s^{-1}) of gaseous fuel in the product layer; $D_{pl,0}$ (m^2 s^{-1}) and Ea_{pl} (kJ mol^{-1}) are the pre-exponential factor and activation energy for the product layer diffusion reaction; k_d, $k_{d,0}$ and Ea_d (kJ mol^{-1}) are the decay constant, pre-exponential factor and activation energy for the product layer diffusivity; R_g denotes the ideal gas constant; T (K) denotes the operation temperature.

The reduction kinetics of Fe_2O_3/Al_2O_3 and $Fe_2O_3/Al_2O_3/TiO_2$ with carbon monoxide were regressed and calculated by the shrinking core model (SCM), as described in Eqs. (7)–(12). After fitting the conversion curves, the kinetic parameters were summarized in Table 3. The mass transfer coefficient (k_g) of around 0.16 mm s^{-1} was calculated for the reduction of Fe_2O_3/Al_2O_3 with carbon monoxide, while the k_g of $Fe_2O_3/Al_2O_3/TiO_2$ for carbon monoxide combustion reached 0.22 mm s^{-1}, indicating that the reaction rate of carbon monoxide for $Fe_2O_3/Al_2O_3/TiO_2$ reduction was faster than that for Fe_2O_3/Al_2O_3 reduction. Less $D_{pl,0}$ was obtained for experiments with Fe_2O_3/Al_2O_3 oxygen carriers than those with $Fe_2O_3/Al_2O_3/TiO_2$ oxygen carriers, explicitly demonstrating that the carbon monoxide more easily diffused through the product layer of $Fe_2O_3/Al_2O_3/TiO_2$ oxygen carriers. Similar results were also observed for Fe_2O_3/Al_2O_3 and $Fe_2O_3/Al_2O_3/TiO_2$ reduction conducted with same operating temperature, as shown in Fig. 3, because the activation energies for the product layer diffusion reaction (Ea_{pl}) were respectively determined to be 255.35 kJ mol^{-1} and 265.91 kJ mol^{-1} for Fe_2O_3/Al_2O_3 and $Fe_2O_3/Al_2O_3/TiO_2$ reduction with CO. For experiments conducted at operating temperature ranged from 875 to 925°C, the decay constants (k_d) of Fe_2O_3/Al_2O_3 and $Fe_2O_3/Al_2O_3/TiO_2$ were determined to be in the range of 7.8 to 10.1 and 12.7 to 14.2, respectively. Higher k_d was obtained for experiments with $Fe_2O_3/Al_2O_3/TiO_2$ particles than those with Fe_2O_3/Al_2O_3 particles, demonstrating that the D_e of $Fe_2O_3/Al_2O_3/TiO_2$ oxygen carriers was more easily depended on the oxygen carrier conversion. Hence, for experiments conducted with the conversion of $Fe_2O_3/Al_2O_3/TiO_2$ oxygen carrier higher than 33.33%, the slope of the reduction conversion vs. time curves was found to be significantly decreased. Furthermore, the slope of the reduction conversion vs. time curves was observed to be slightly altered for experiments conducted at various operating temperature, which might be also attributed to the decay constant (k_d) was dependent on the operating temperatures, consistent with the result found in literature (de Diego *et al.*, 2014; Abad *et al.*, 2015). For experiments conducted with an operating temperature of 900°C, the slope of the Fe_2O_3/Al_2O_3 reduction conversion vs. time curves were changed with inlet CO concentration ranged from 5 to 20%, as shown in Fig. 4, possibly due to high $k_{d,0}$ was obtained for Fe_2O_3/Al_2O_3 reduction with CO (Cabello *et al.*, 2014).

Charcoal Gasification with Steam in an Empty Bed Reactor

Steam was employed to be a gasification agent, and the main mechanism of the charcoal gasification in the steam-containing gaseous stream could be described as the following (Gayán *et al.*, 2010; Cuadrat *et al.*, 2011; Wu *et al.*, 2015):

$$Charcoal \rightarrow Volatile\ matter + Char \quad (13)$$

$$C_nH_m + nH_2O \leftrightarrow \left(n+\frac{m}{2}\right)H_2 + nCO \quad (14)$$

$$CO + H_2O \rightarrow CO_2 + H_2 \quad (15)$$

$$Char + H_2O \rightarrow CO + H_2 + Ash \quad (16)$$

Table 3. Kinetics parameters for the reduction of iron-based oxygen carriers conducted with CO.

Parameter	Symbol	Unit	Fe_2O_3/Al_2O_3	$Fe_2O_3/Al_2O_3/TiO_2$
Mass transfer coefficient	k_g	mm s^{-1}	0.16	0.22
Pre-exponential factor for the product layer diffusion reaction	$D_{pl,0}$	mm^2 s^{-1}	1.34×10^{11}	9.09×10^{11}
Activation energy for the product layer diffusion reaction	E_{pl}	kJ mol^{-1}	255.35	265.91
Pre-exponential factor for the product layer diffusivity	$k_{d,0}$	–	3737.23	162.86
Activation energy for the product layer diffusivity	E_d	kJ mol^{-1}	58.91	24.34

The concentrations of the gaseous products for the gasification of charcoal by steam at various operating temperature are shown in Fig. 5. Elevated operating temperature increased the CO concentration, whereas diminished the CO_2 and CH_4 concentrations. It is ascribed that the endothermic reactions (steam reforming reaction and char gasification) are favorably occurred at higher operating temperature, instead the exothermic reaction (water gas shift reaction) is not favorable (Chiu *et al.*, 2014b). In addition, the H_2 concentration was slightly declined with the operating temperature between 850°C and 900°C, due to the less volatile matter contained in charcoal. Fig. 6 shows the gaseous product concentrations during charcoal gasification at various steam flow rate.

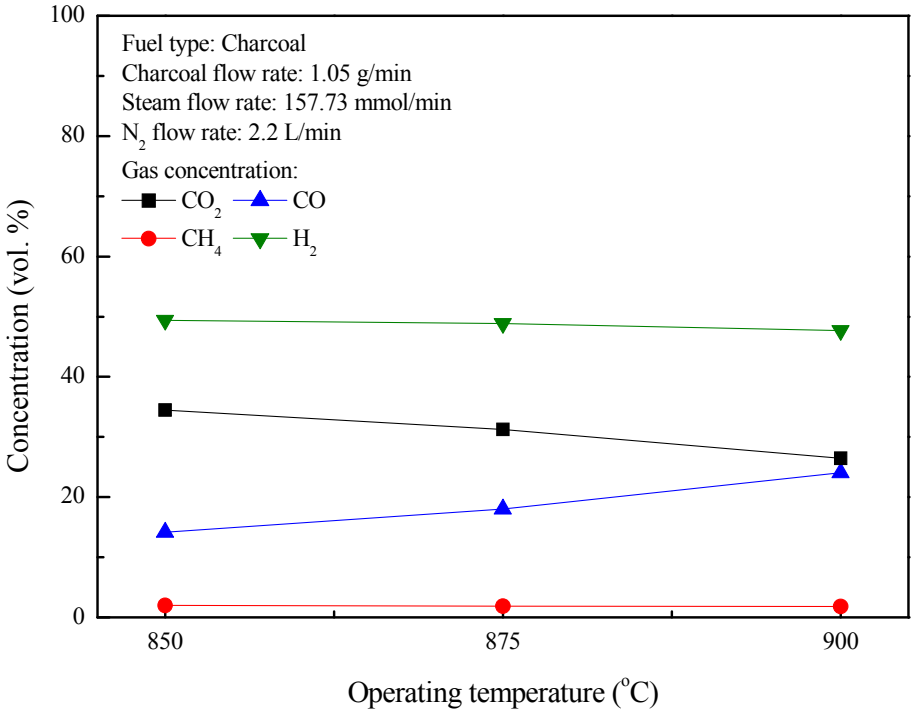

Fig. 5. Effect of operating temperature on the gasification of charcoal in the empty bed.

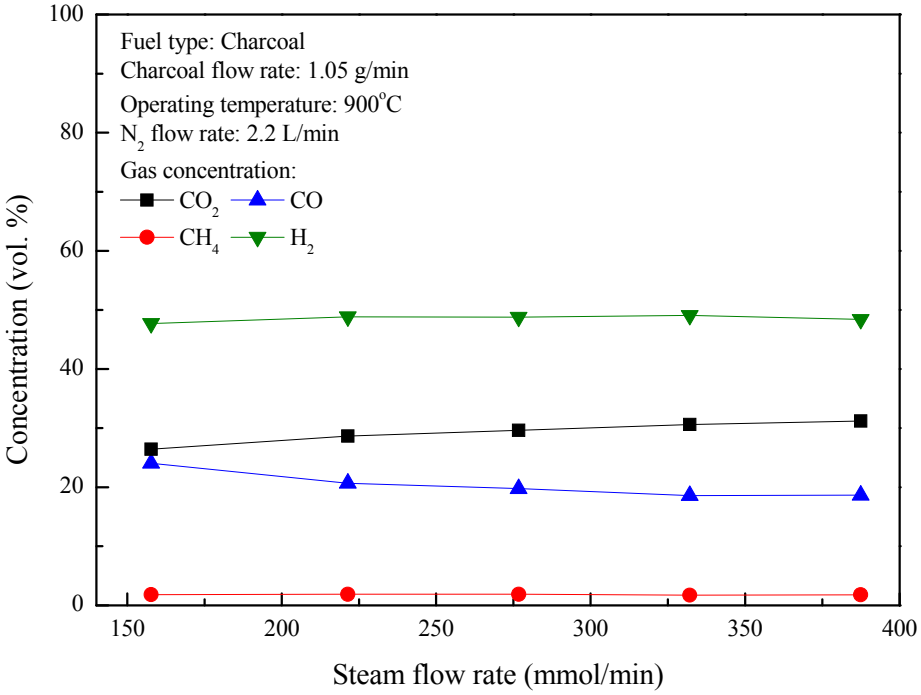

Fig. 6. Effect of steam flow rate on the gasification of charcoal in the empty bed.

Increased steam flow rate diminished the CO and CH_4 concentrations, whereas enhanced the CO_2 and H_2 concentrations. Experiments conducted with high steam flow rate might be beneficial for steam reforming reaction and water gas shift reaction.

CLC of Charcoal by Fe_2O_3/Al_2O_3 Particles

A series of experiments were carried out to study the CLC of charcoal by Fe_2O_3/Al_2O_3 particles. Results for experiments conducted at different steam flowrates are presented in Fig. 7. The maximum concentration of CO_2 was obtained at inlet steam flowrate of 157.7 mmol min^{-1}. The result implied that the combustible gaseous products (H_2, CO, and CH_4) generated from charcoal gasification were completely combusted by the oxygen carrier. However, the CO_2 concentration was significantly dwindled by increasing the steam flowrate. The enhancement of H_2 and CO concentrations could be attributed to the incomplete combustion of fuel gas generated from charcoal gasification. The carbon conversion (X_C) and the oxygen carrier conversion (X_{OC}) for charcoal combustion were determined using the following relationship:

$$X_C = \frac{F_{CO_2} + F_{CO} + F_{CH_4}}{F_{C,in}} \tag{17}$$

$$X_{OC} = \frac{\left(2F_{CO_2} + F_{CO} + F_{H_2O} + F_{O,out}\right) - \left(F_{O,in} + F_{H_2O,in}\right)}{\left(\frac{x_{Fe_2O_3} \cdot \dot{m}_{OC}}{M_{Fe_2O_3}}\right) \times 1000 \times 3} \tag{18}$$

$$\dot{m}_{Charcoal,out} = \dot{m}_{Charcoal,in}\left(1 - X_C\right) \tag{19}$$

$$F_{H_2O} = \left(0.5F_{H,in} + F_{H_2O,in}\right) - \left(0.5F_{H,out} + F_{H_2} + F_{CH_4}\right) \tag{20}$$

$$F_{H,out} = \frac{2.11\% \times \dot{m}_{Charcoal,out}}{M_H} \times 1000 \tag{21}$$

$$F_{O,out} = \frac{2.69\% \times \dot{m}_{Charcoal,out}}{M_O} \times 1000 \tag{22}$$

where F_i is the effluent molar flowrate (mmol min^{-1}) of species i; i is denoted as CO_2, CO, H_2O, H_2 and CH_4; $F_{C,in}$, $F_{H,in}$ and $F_{O,in}$ are the inlet carbon, hydrogen and oxygen mole flow rate (mmol min^{-1}) of charcoal, respectively; $F_{O,out}$ and $F_{H,out}$ are the outlet oxygen and hydrogen mole flow rate (mmol min^{-1}) of unburned charcoal, respectively; $F_{H_2O,in}$ is the inlet mole flow rate (mmol min^{-1}) of H_2O; $\dot{m}_{Charcoal,in}$ and $\dot{m}_{Charcoal,out}$ are the inlet and outlet mass flow rate (g min^{-1}) of charcoal; $\dot{m}_{OC}$ is the mass flow rate (g min^{-1}) of the oxygen carriers in the ADMBR. Fig. 8 shows the effect of inlet steam flow rate on the combustion of charcoal by the CLC process with Fe_2O_3/Al_2O_3 oxygen carriers in the ADMBR operated at 900°C. For steam feeding rate more than 157.7 mmol min^{-1}, the carbon conversion was retained to about 60%, indicating that charcoal gasification was not significantly enhanced with the application of more steam, due to charcoal gasification is the limiting step, consistent with the data found in the literature (Luo *et al.*, 2014b). Hence, the longer residence time is required

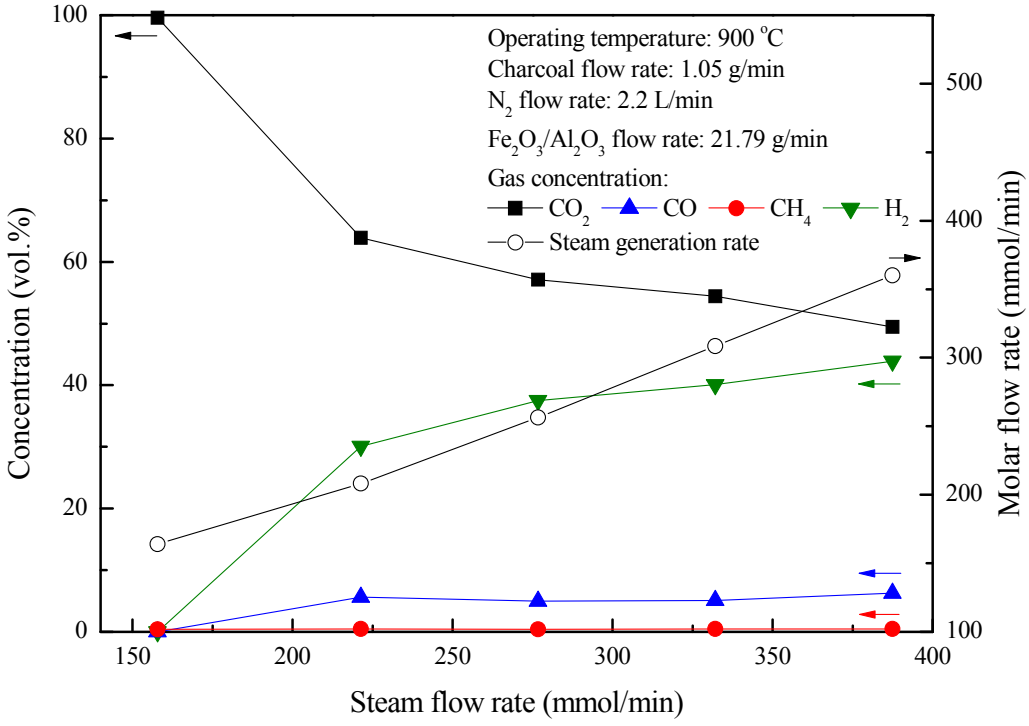

Fig. 7. Effect of steam flow rates on the combustion of charcoal with Fe_2O_3/Al_2O_3 in the moving bed.

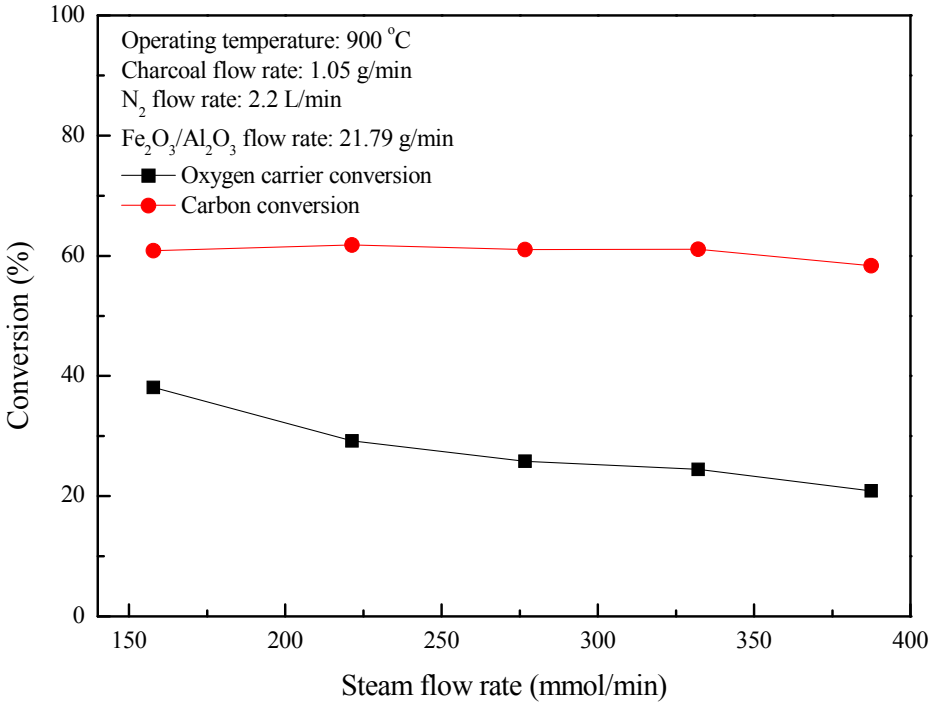

Fig. 8. Effect of steam flow rates on fuel and oxygen carrier conversions for CLC of charcoal with Fe_2O_3/Al_2O_3 in the moving bed.

for the gasification of charcoal occurred in the fuel reactor. Experimental results illustrated in Fig. 8 also exhibited that the almost complete reaction between Fe_2O_3/Al_2O_3 oxygen carriers and fuel gases generated from the charcoal gasification could be accomplished for the experiment conducted with inlet steam flow rate of 157.7 mmol min^{-1}. However, as for experiments conducted with carbon conversion of about 60%, the effluent concentrations of H_2 and CO were enhanced with steam feeding rate ranged from 221.4 to 387.4 mmol min^{-1}, because of the insufficient residence time was provided for the CLC of fuel gases with Fe_2O_3/Al_2O_3 particles. As also indicated in Fig. 8, the maximum conversion of Fe_2O_3/Al_2O_3 particles (nearly 38%) was obtained for the combustion of charcoal with inlet steam flow rate of 157.7 mmol min^{-1}, demonstrating the component of reduced oxygen carriers was majorly FeO, consistent with the result found in the literature (Luo *et al.*, 2014b). Nevertheless, the oxygen carrier conversions of Fe_2O_3/Al_2O_3 particles were found to decrease with increasing inlet steam flowrate, because less Fe_2O_3/Al_2O_3 oxygen carriers were considered to be reduced by fuel gases, such as CH_4, CO, and H_2, which is generated by char gasification and combustion.

CLC of Charcoal by $Fe_2O_3/Al_2O_3/TiO_2$ Particles

CLC experiments were conducted in this study to examine the combustion of charcoal under various inlet steam flow rate. As the experimental results illustrated in Fig. 9, outlet gas stream containing about 99% CO_2 and 1% CH_4 were achieved for experiments with inlet steam flowrate operated between 157.7 mmol min^{-1} and 221.4 mmol min^{-1}, but the effluent concentration of CO_2 was dropped for experiments carried out with inlet steam flow rate of 276.7 mmol min^{-1}. These experimental observations may be attributed due to more combustible gas (CH_4, H_2, and CO) generated by Eqs. (13)–(16) were higher than that consumed by $Fe_2O_3/Al_2O_3/TiO_2$ reduction reaction. Further increases of inlet steam flow rate (> 276.7 mmol min^{-1}), however, could enhance the CO_2 and CH_4 effluent concentrations, and decrease the H_2 and CO effluent concentrations. The only slightly enhanced methane concentration may be ascribed to the low reactivity of the iron-based oxygen carriers with methane. The injections of excessive steam inhibited charcoal gasification due to insufficient residence time was provided. Thus, less charcoal was gasified to generate methane, hydrogen and carbon monoxide, and then hydrogen and carbon monoxide were further combusted with $Fe_2O_3/Al_2O_3/TiO_2$ oxygen carrier to generate carbon dioxide and steam. Besides, fewer H_2 and CO outlet concentration were observed for charcoal combustion with $Fe_2O_3/Al_2O_3/TiO_2$ particle than those with Fe_2O_3/Al_2O_3 particle, because of the hydrogen and carbon monoxide were considered to be consumed more rapidly by $Fe_2O_3/Al_2O_3/TiO_2$ reduction reaction than by Fe_2O_3/Al_2O_3 reduction reaction. Fig. 10 shows that carbon conversions were obviously increased for charcoal combustion conducted with 7.5 g min^{-1} $Fe_2O_3/Al_2O_3/TiO_2$ particles, and inlet steam flow rate ranged from 157.7 to 221.4 mmol min^{-1}. Luo *et al.* (2014b) indicated that the kinetic of charcoal gasification was enhanced by increasing the flow rate of the gasification agent. More H_2O and CO_2 were produced from fuel gases combustion and was subsequently reacted with charcoal to perform gasification reaction, consistent with the results found in the literatures

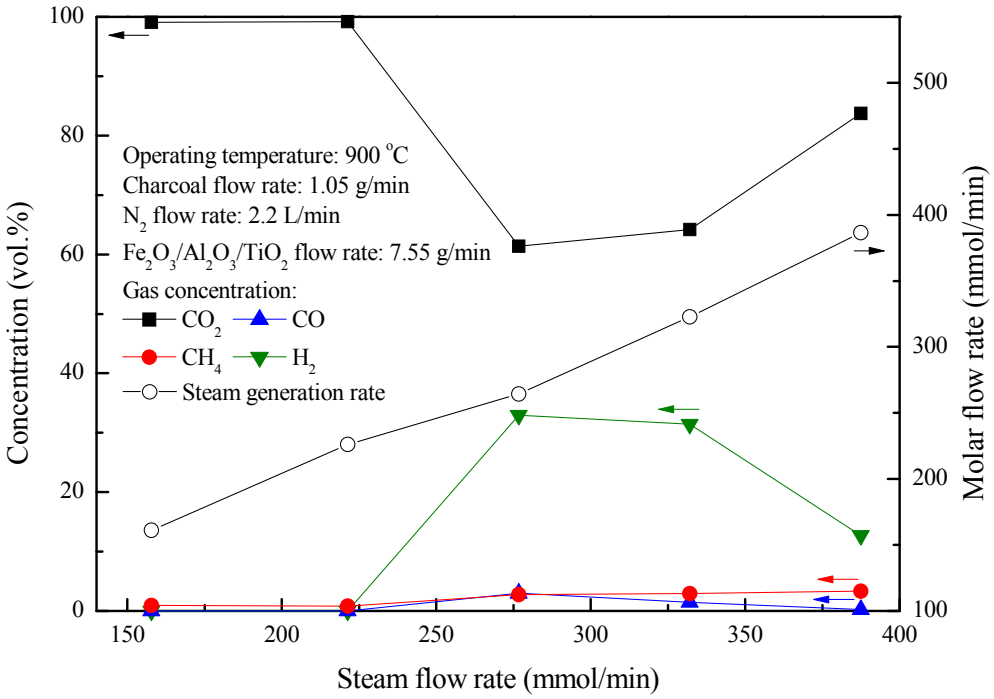

Fig. 9. Effect of steam flow rates on the combustion of charcoal with $Fe_2O_3/Al_2O_3/TiO_2$ in the moving bed.

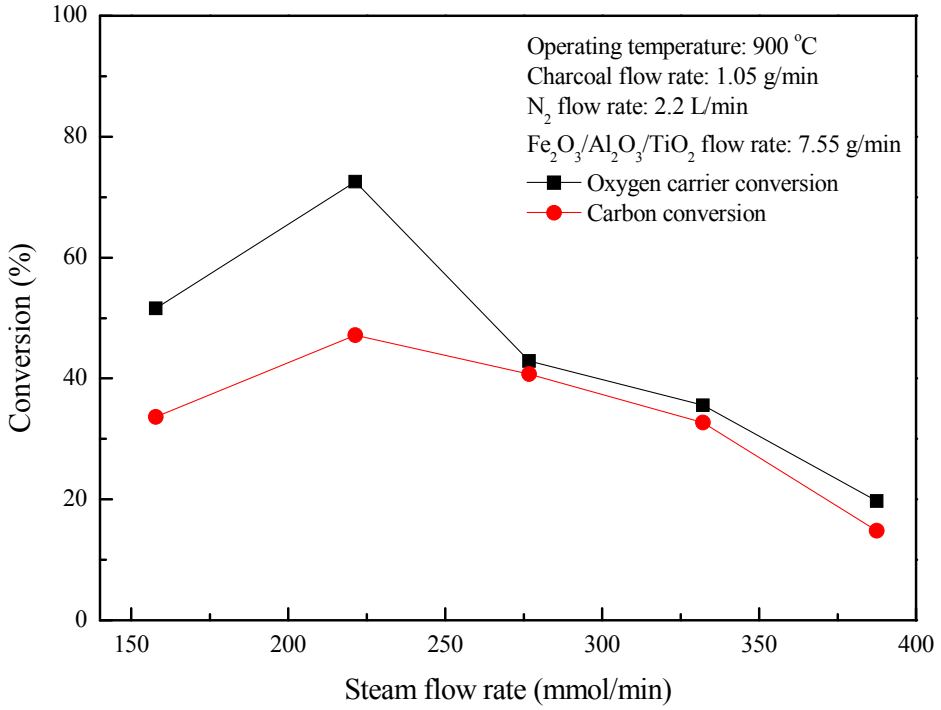

Fig. 10. Effect of steam flow rates on fuel and oxygen carrier conversions for CLC of charcoal with $Fe_2O_3/Al_2O_3/TiO_2$ in the moving bed.

(Fan, 2010; Wu and Ku, 2016). However, the carbon conversions were found to be diminished by the addition of excessive steam (> 221.4 mmol min^{-1}). The carbon conversions were decreased for CLC of charcoal is possibly caused by the fuel gases not immediately combusted with $Fe_2O_3/Al_2O_3/TiO_2$ oxygen carriers, and more H_2 and CO were presented in the fuel reactor effluent. As shown in Figs. 8 and 10, maximum carbon conversion of around 61.8% was achieved for charcoal combustion with Fe_2O_3/Al_2O_3, while the maximum carbon conversion of charcoal combustion with $Fe_2O_3/Al_2O_3/TiO_2$ reached about 47.2% for experiments conducted with inlet steam flow rate of

221.4 mmol min^{-1}, indicating insufficient oxygen was provided to fully combust charcoal. Fewer carbon conversions were observed for the combustion of charcoal with $Fe_2O_3/Al_2O_3/TiO_2$ than that for charcoal combustion with Fe_2O_3/Al_2O_3, further demonstrating charcoal gasification was impeded because the amount of $Fe_2O_3/Al_2O_3/TiO_2$ mass flow for charcoal combustion was lower than that of Fe_2O_3/Al_2O_3 mass flow.

Fig. 10 reveals the X_{OC} of $Fe_2O_3/Al_2O_3/TiO_2$ particles were enhanced for experiments conducted with inlet steam flow rate ranged from 157.7 to 221.4 mmol min^{-1}, demonstrating increased steam flow rate to promote the charcoal gasification, and further enhance the $Fe_2O_3/Al_2O_3/TiO_2$ reduction. Subsequently, the oxygen carrier conversion was markedly dropped with inlet steam flow rate ranged from 221.4 to 387.4 mmol min^{-1}, indicating not enough residence time was provided to reduce $Fe_2O_3/Al_2O_3/TiO_2$ oxygen carriers with the fuel gases generated by char gasification and combustion. Thus, experiments conducted with excessive inlet steam flow rate might not be favorable to perform iron-based oxygen carrier reduction. Less oxygen carrier was demanded for the combustion of charcoal with $Fe_2O_3/Al_2O_3/TiO_2$ than that for charcoal combustion with Fe_2O_3/Al_2O_3, probably because lattice oxygen present in the $Fe_2O_3/Al_2O_3/TiO_2$ oxygen carriers are more ready to react with combustible gas, especially hydrogen and carbon monoxide. Moreover, fewer oxygen carriers are required may also be ascribed to the higher Fe_2O_3 contained in the $Fe_2O_3/Al_2O_3/TiO_2$ oxygen carrier. Abad *et al.* (2007) analyzed the design criteria for a CLC system and reported that the solid circulation rate was decreased with increasing the metal oxide content for the combustion of fuel gases (H_2, CO, and CH_4) with different metal oxides (CuO, NiO, and Fe_2O_3).

Crystalline Phase Identification and Heat Analysis

The XRD diffraction peaks of prepared Fe_2O_3/Al_2O_3 particles for the crystal-phase transformation are presented in Fig. 11, indicating that only Fe_2O_3 and Al_2O_3 are found for fresh oxygen carriers. However, the crystal phases of the reduced Fe_2O_3/Al_2O_3 particles identified from the XRD spectra can be classified into three components of Al_2FeO_4, Fe_3O_4, and Al_2O_3, indicating that the amount of oxygen utilization from F_2O_3 to slightly Fe_3O_4 and FeO. A similar observation was obtained by Ishida *et al.* (2005) and Ku *et al.* (2014). Zhu *et al.* (2016) analyzed the atomic structural evolution during the reduction of α-Fe_2O_3 nanowires and also reported that more oxygen vacancies were formed as the reduction continues. Thus, the rhombohedral structure of α-Fe_2O_3 become unstable and transformed into the cubic structure of Fe_3O_4. In this study, Fe_3O_4 was further reduced to form the cubic structure of Al_2FeO_4. Few Fe_3O_4 was observed in the reduced Fe_2O_3/Al_2O_3 particles possibly due to the presence of insufficient residence time. Subsequently, the reduced Fe_2O_3/Al_2O_3 oxygen carriers were completely oxidized by air to generate Fe_2O_3 and Al_2O_3, which were observed in the XRD pattern.

As shown in Fig. 12, Fe_2O_3, Fe_2TiO_5 and Al_2O_3 were the major crystalline phases of fresh $Fe_2O_3/Al_2O_3/TiO_2$ oxygen carriers. For an experiment conducted with inlet steam flow rate of 387.4 mmol min^{-1} and $Fe_2O_3/Al_2O_3/TiO_2$ flow

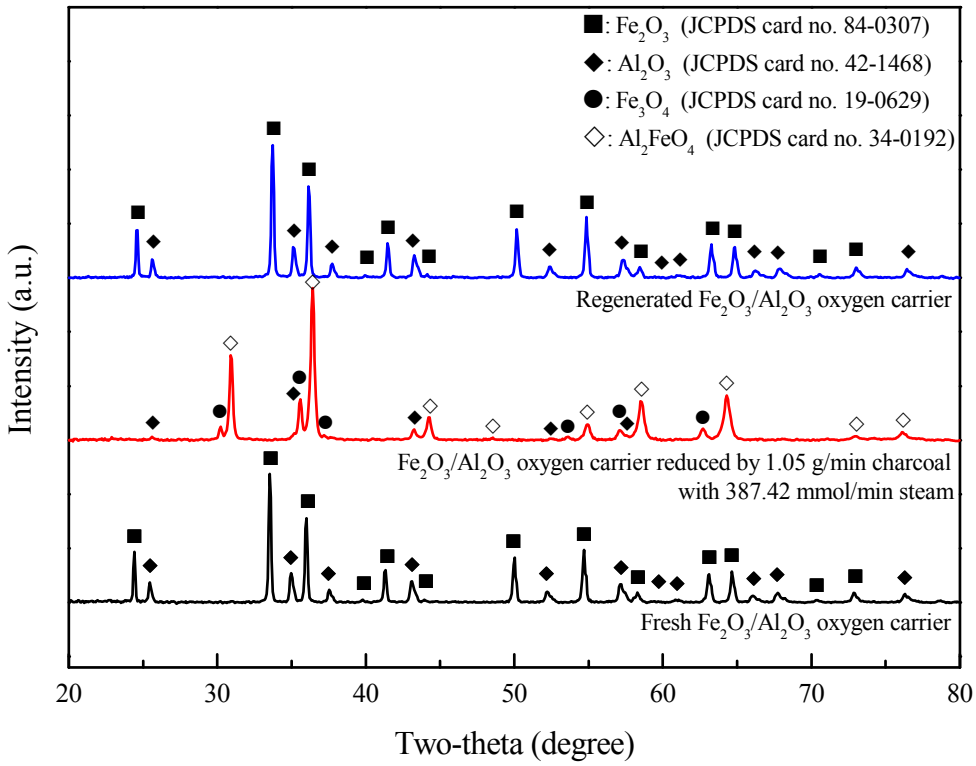

Fig. 11. X-ray diffraction patterns of fresh, reduced and regenerated Fe_2O_3/Al_2O_3 oxygen carriers for charcoal combustion.

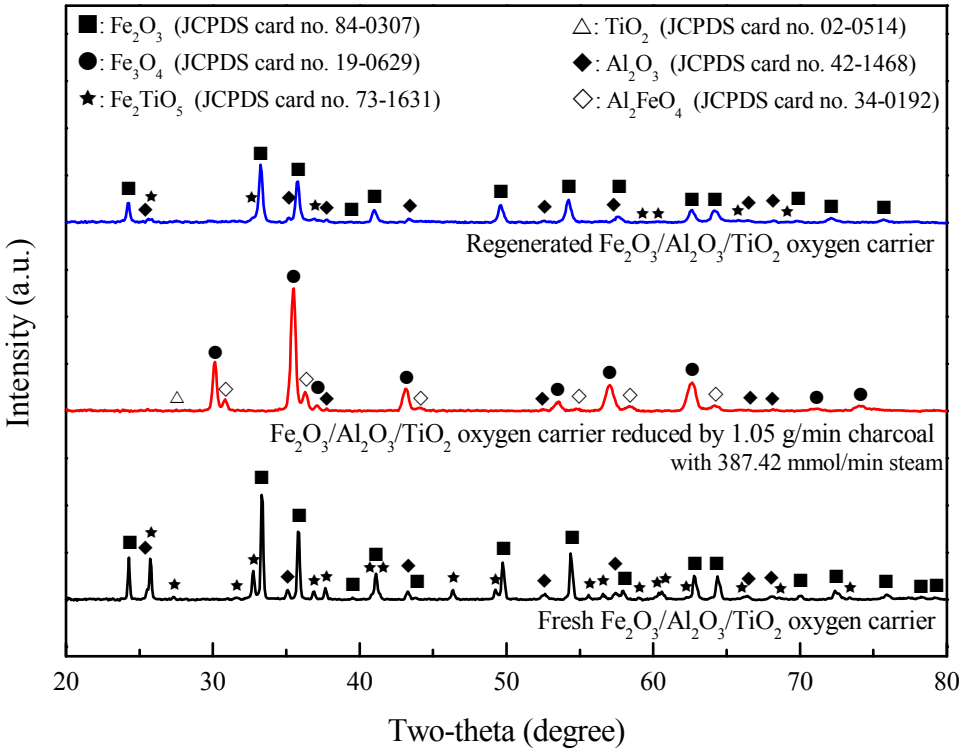

Fig. 12. X-ray diffraction patterns of fresh, reduced and regenerated $Fe_2O_3/Al_2O_3/TiO_2$ oxygen carriers for charcoal combustion.

rate of 7.55 g min^{-1}, the reduced $Fe_2O_3/Al_2O_3/TiO_2$ oxygen carriers were sampled from moving bed operation. The absence of Fe_2O_3 and Fe_2TiO_5 in the XRD pattern indicated that Fe_2O_3 and Fe_2TiO_5 were completely reduced. Hence, the rhombohedral structure of α-Fe_2O_3 and the orthorhombic structure of Fe_2TiO_5 were transformed into the cubic structure of Fe_3O_4 and Al_2FeO_4, as illustrated in Fig. 12. Similar results were obtained in the investigation of Abad *et al.* (2011) and Zhu *et al.* (2016). For $Fe_2O_3/Al_2O_3/TiO_2$ oxygen carriers sampled after regeneration, Fe_2O_3, Fe_2TiO_5, and Al_2O_3 were observed in the XRD pattern, demonstrating that Fe_3O_4, Al_2FeO_4, Al_2O_3 and slightly TiO_2 contained in the reduced $Fe_2O_3/Al_2O_3/TiO_2$ oxygen carriers were completely oxidized to Fe_2O_3, Fe_2TiO_5, and Al_2O_3.

The mechanism for reduction of Fe_2O_3/Al_2O_3 and $Fe_2O_3/Al_2O_3/TiO_2$ oxygen carriers with CO or H_2 are proposed as Eqs. (23)–(26) based on the experimental results of this study. Unfortunately, the oxygen carrier conversion contributed by each reduction reactions were not possible to be separated because these reduction reactions may occur simultaneously. Therefore, the overall reduction reaction of iron-based oxygen carrier for methane combustion is summarized and simplified by Integrated Rate of Reduction (IRoR) model, which has been widely used for evaluating the total reduction rate of iron ores (Abad *et al.*, 2011).

For Fe_2O_3/Al_2O_3 reduction:

$$Fe_2O_3 + 2Al_2O_3 + CO/H_2 \leftrightarrow 2Al_2FeO_4 + CO_2/H_2O \quad (23)$$

$$3Fe_2O_3 + CO/H_2 \leftrightarrow 2Fe_3O_4 + CO_2/H_2O \quad (24)$$

For $Fe_2O_3/Al_2O_3/TiO_2$ reduction:

$$Fe_2TiO_5 + TiO_2 + CO/H_2 \leftrightarrow 2Fe_2TiO_3 + CO_2/H_2O \quad (25)$$

$$FeTiO_3 + CO/H_2 \leftrightarrow Fe + TiO_2 + CO_2/H_2O \quad (26)$$

The definition of input processing capacity (Q_{in}) and output processing capacity for charcoal combustion ($Q_{C,out}$) and unburned ($Q_{unC,out}$) are expressed, respectively, as follows:

$$Q_{in} = \dot{m} \cdot \Delta H_{Fuel} \quad (27)$$

$$Q_{C,out} = \sum (F_{j,out,g} - F_{j,out,C}) \cdot \Delta H_{rxn,j} \quad (28)$$

$$Q_{unC,out} = \sum F_{j,out,C} \cdot \Delta H_{rxn,j} \quad (29)$$

where $\dot{m}$ is the charcoal feeding rate (g s^{-1}); ΔH_{Fuel} denotes the higher heating value (MJ kg^{-1}) of charcoal; $F_{j,out,g}$ and $F_{j,out,C}$ are the molar flowrate of combustible species j in the effluent stream such as CO, CH_4, H_2, and C; the combustible species generated from charcoal gasification and combustion are denoted as g and C; $\Delta H_{rxn,j}$ denotes the heat of combustion of species j. The output processing capacity for charcoal gasification ($Q_{g,out}$) was calculated by the heat balance, as described by Eq. (30):

$$Q_{in} = Q_{g,out} + Q_{C,out} + Q_{unC,out} \quad (30)$$

As revealed in Fig. 13, $Q_{g,out}$ for the combustion of charcoal with Fe_2O_3/Al_2O_3 and $Fe_2O_3/Al_2O_3/TiO_2$ oxygen

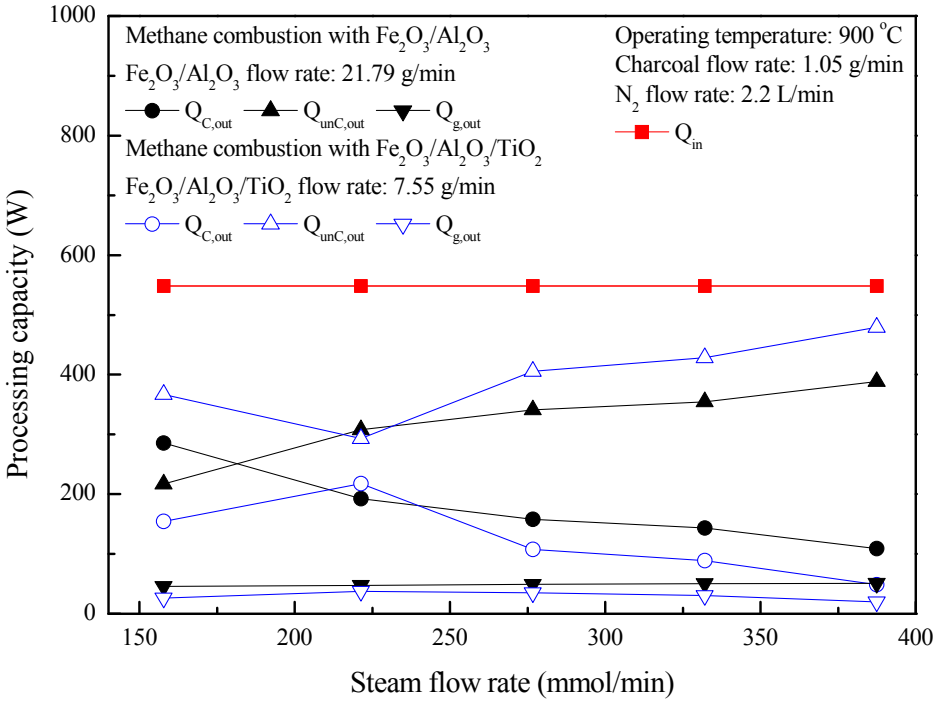

Fig. 13. Effect of steam flow rate on processing capacity for charcoal combustion in the moving bed.

carriers were determined to be roughly 49 W and 30 W, respectively, further demonstrating that roughly 9% and 5% of Q_{in} released for full charcoal decomposition in the ADMBR. A maximum value of output processing capacity for charcoal combustion with Fe_2O_3/Al_2O_3 oxygen carriers was estimated to be 285 W as CO_2 concentration reached nearly 100%. Afterward, $Q_{C,out}$ was gradually decreased with the increase of steam feeding rate. Moreover, $Q_{C,out}$ of charcoal combustion by $Fe_2O_3/Al_2O_3/TiO_2$ oxygen carriers increased as steam feeding rate increased from 157.7 to 221.4 mmol min^{-1}, and reached around 217 W as CO_2 concentration reached 99%, as shown in Fig. 13. However, $Q_{C,out}$ decreased obviously with increasing inlet steam flow rate and reduced to around 49 W, indicating that the excessive amount of steam might be negative for burning the charcoal with iron-based oxygen carriers. The heat release of charcoal combustion using the Fe_2O_3/Al_2O_3 particles was more than that of using the $Fe_2O_3/Al_2O_3/TiO_2$ particles because the high feeding rate of Fe_2O_3/Al_2O_3 was provided. It should be pointed out that although the oxygen carrier flow rate of $Fe_2O_3/Al_2O_3/TiO_2$ only operated at 7.55 g min^{-1}, practically 255 W (about 46% of Q_{in}) was released for the combustion of charcoal by using $Fe_2O_3/Al_2O_3/TiO_2$, probably because combustible gases were more ready to react with the Fe_2O_3 contained in the $Fe_2O_3/Al_2O_3/TiO_2$ oxygen carriers.

CONCLUSIONS

Fe_2O_3 supported by Al_2O_3 and Al_2O_3/TiO_2 was investigated as an oxygen carrier for the CLC of charcoal. The kinetics of reducing Fe_2O_3/Al_2O_3 and $Fe_2O_3/Al_2O_3/TiO_2$ with hydrogen were well described by a shrinking core model. The results indicated that the $Fe_2O_3/Al_2O_3/TiO_2$ was reduced more quickly than the Fe_2O_3/Al_2O_3 by carbon monoxide, which diffused more easily through the product layer of the former. When the inlet steam flow rate was set to 221.4 mmol min^{-1}, approximately 61.8% and 47.2% of the charcoal was combusted in the moving bed reactor with Fe_2O_3/Al_2O_3 and $Fe_2O_3/Al_2O_3/TiO_2$, respectively; additionally, these oxygen carriers achieved conversion rates of ~29.2% and ~72.5%, respectively. Based on the XRD characterization, a phase transformation from Fe_2O_3 (rhombohedral) and/or Fe_2TiO_5 (orthorhombic) to Fe_3O_4 (cubic) and Al_2FeO_4 (cubic) occurred during the CLC of charcoal. Because a high flow rate was used for Fe_2O_3/Al_2O_3, more heat was released when the charcoal was combusted with this oxygen carrier than with $Fe_2O_3/Al_2O_3/TiO_2$. Furthermore, the $Fe_2O_3/Al_2O_3TiO_2$ particles reacted strongly to syngas (CO–H_2) due to their abundant Fe_2O_3 content; hence, less $Fe_2O_3/Al_2O_3/TiO_2$ was needed for combusting the charcoal.

ACKNOWLEDGMENTS

The authors would like to thank the Ministry of Science and Technology of the Republic of China (Taiwan) for financially supporting this research under Contract No. MOST 106-3113-E-007-002-. The contribution on the supply of hematite powders by China Steel Corp. is gratefully acknowledged.

REFERENCES

Abad, A., Adánez, J., García-Labiano, F., de Diego, L.F., Gayán, P. and Celaya, J. (2007). Mapping of the range of operational conditions for Cu-, Fe-, and Ni-based

oxygen carriers in chemical-looping combustion. *Chem. Eng. Sci.* 62: 533–549.

Abad, A., Adánez, J., Cuadrat, A., García-Labiano, F., Gayán, P. and de Diego, L.F. (2011). Kinetics of redox reactions of ilmenite for chemical-looping combustion. *Chem. Eng. Sci.* 66: 689–702.

Abad, A., García-Labiano, F., Gayán, P., de Diego, L.F. and Adánez, J. (2015). Redox kinetics of $CaMg_{0.1}Ti_{0.125}Mn_{0.775}O_{2.9-\delta}$ for Chemical Looping Combustion (CLC) and Chemical Looping with Oxygen Uncoupling (CLOU). *Chem. Eng. J.* 269: 67–81.

Adánez, J., Cuadrat, A., Abad, A., Gayán, P., de Diego, L.F. and García-Labiano, F. (2010). Ilmenite activation during consecutive redox cycles in chemical-looping combustion. *Energy Fuels* 24: 1402–1413.

Adánez, J, Abad, A, Garcia-Labiano, F, Gayan, P and de Diego, L.F. (2012). Progress in chemical-looping combustion and reforming technologies. *Prog. Energy Combust. Sci.* 38: 215–282.

Bayham, S.C., Kim, H.R., Wang, D., Tong, A., Zeng, L., McGiveron, O., Kathe, M.V., Chung, E., Wang, W., Wang, A., Majumder, A. and Fan, L.S. (2013). Iron-based coal direct chemical looping combustion process: 200-h continuous operation of a 25-kW_{th} subpilot unit. *Energy Fuels* 27: 1347–1356.

Berguerand, N. and Lyngfelt, A. (2008). Design and operation of a 10 kW_{th} chemical-looping combustor for solid fuels - testing with South African coal. *Fuel* 87: 2713–2726.

Breault, R.W., Yarrington, C.S. and Weber, J.M. (2016). The effect of thermal treatment of hematite ore for chemical looping combustion of methane. *J. Energy Resour. Technol.* 138: 0422021–0422028.

Cabello, A., Abad, A., García-Labiano, F., Gayán, P., de Diego, L.F. and Adánez, J. (2014). Kinetic determination of a highly reactive impregnated Fe_2O_3/Al_2O_3 oxygen carrier for use in gas-fueled chemical looping combustion. *Chem. Eng. J.* 258: 265–280.

Cao, Y., Sit, S.P. and Pan, W.P. (2014). Preparation and characterization of lanthanum-promoted copper-based oxygen carriers for chemical looping combustion process. *Aerosol Air Qual. Res.* 14: 572–584.

Chiu, P.C. and Ku, Y. (2012). Chemical looping process-a novel technology for inherent CO_2 capture. *Aerosol Air Qual. Res.* 12: 1421–1432.

Chiu, P.C., Ku, Y., Wu, Y.L., Wu, H.C., Kuo, Y.L. and Tseng, Y.H. (2014a). Characterization and evaluation of prepared Fe_2O_3/Al_2O_3 oxygen carriers for chemical looping process. *Aerosol Air Qual. Res.* 14: 981–990.

Chiu, P.C., Ku, Y., Wu, H.C., Kuo, Y.L. and Tseng, Y.H. (2014b). Spent isopropanol solution as possible liquid fuel for moving bed reactor in chemical looping combustion. *Energy Fuels* 28: 657–665.

Cuadrat, A., Abad, A., García-Labiano, F., Gayán, P., de Diego, L.F. and Adánez, J. (2011). The use of ilmenite as oxygen-carrier in a 500Wth chemical-looping coal combustion unit. *Int. J. Greenhouse Gas Control* 5: 1630–1642.

de Diego, L.F., Abad, A., Cabello, A., Gayán, P., García-Labiano, F. and Adánez, J. (2014) Reduction and oxidation kinetics of a $CaMn_{0.9}Mg_{0.1}O_{3-\delta}$ oxygen carrier for chemical-looping combustion. *Ind. Eng. Chem. Res*. 53: 87–103.

Dharanipragada, N.V.R.A., Galvita, V.V., Poelman, H., Buelens, L.C. and Marin, G.B. (2017). Insight in kinetics from pre-edge features using time resolved in situ XAS. *AlChE J.* 64: 1339–1349.

Fan, L.S. (2010). *Chemical looping systems for fossil energy conversions*. John Wiley & Sons, Inc., New York.

Fan, L.S., Zeng, L. and Luo, S. (2015). Chemical-looping technology platform. *AIChE J.* 61: 2–22.

Frick, V., Rydén, M. and Leion, H. (2016). Investigation of Cu–Fe and Mn–Ni oxides as oxygen carriers for chemical-looping combustion. *Fuel Process. Technol.* 150: 30–40.

Gao, Z.F., Wu, Z.J. and Liu, W.M. (2016). Preparation and chemical looping combustion properties of Fe_2O_3/Al_2O_3 derived from metallurgy iron-bearing dust. *J. Environ. Chem. Eng.* 4: 1653–1663.

Gayán, P., Forero, C.R., de Diego, L.F., Abad, A., García-Labiano, F. and Adánez, J. (2010). Effect of gas composition in chemical-looping combustion with copper-based oxygen carriers: Fate of light hydrocarbons. *Int. J. Greenhouse Gas Control* 4: 13–22.

Gu, H., Shen, L., Xiao, J., Zhang, S. and Song, T. (2011). Chemical looping combustion of biomass/coal with natural iron ore as oxygen carrier in a continuous reactor. *Energy Fuels* 25: 446–455.

Gu, H., Shen, L., Zhong, Z., Niu, X., Ge, H., Zhou, Y. and Xiao, S. (2014). Potassium-modified iron ore as oxygen carrier for coal chemical looping combustion: Continuous test in 1 kW reactor. *Ind. Eng. Chem. Res.* 53: 13006–13015.

Gucho, E.M., Shahzad, K., Bramer, E.A., Akhtar, N.A. and Brem, G. (2015). Experimental study on dry torrefaction of beech wood and miscanthus. *Energies* 8: 3903–3923.

Huang, Z., Zhang, Y., Fu, J., Yu, L., Chen, M., Liu, S., He, F., Chen, D., Wei, G., Zhao, K., Zheng, A., Zhao, Z. and Li, H. (2016). Chemical looping gasification of biomass char using iron ore as an oxygen carrier. *Int. J. Hydrogen Energy* 41: 17871–17883.

International Energy Agency (IEA) (2009). *Coal Information 2009 Edition Documentation for Beyond 2020 Files*. IEA, Paris, France.

Ishida, M., Takeshita, K., Suzuki, K. and Ohba, T. (2005). Application of Fe_2O_3-Al_2O_3 composite particles as solid looping material of the chemical-loop combustor. *Energy Fuels* 19: 2514–2518.

Ismail, M., Liu, W. and Scott, S.A. (2013). The performance of Fe_2O_3-CaO oxygen carriers and the interaction of iron oxides with CaO during chemical looping combustion and H_2 production. *Energy Procedia* 63: 87–97.

Kim, H.R., Wang, D., Zeng, L., Bayham, S., Tong, A., Chung, E., Kathe, M.V., Luo, S., McGiveron, O., Wang, A., Sun, Z., Chen, D. and Fan, L.S. (2013). Coal direct chemical looping combustion process: Design and operation of a 25-kW_{th} sub-pilot unit. *Fuel* 108: 370–384.

Ksepko, E., Babinski, P., Evdou, A. and Nalbandian, L. (2016). Studies on the redox reaction kinetics of selected, naturally occurring oxygen carrier. *J. Therm. Anal. Calorim.* 124: 137–150.

Ksepko, E., Babinski, P. and Nalbandian, L. (2017). The redox reaction kinetics of Sinai ore for chemical looping combustion applications. *Appl. Energy* 190: 1258–1274.

Ku, Y., Wu, H.C., Chiu, P.C., Tseng, Y.H. and Kuo, Y.L. (2014). Methane combustion by moving bed fuel reactor with Fe_2O_3/Al_2O_3 oxygen carriers. *Appl. Energy* 113: 1909–1915.

Ku, Y., Lin, P.H., Wu, H.C., Liu, Y.C., Tseng, Y.H. and Lee, H.Y. (2017). Preparation of Fe_2O_3/Al_2O_3 and Fe_2O_3/TiO_2 pellets as oxygen carrier for chemical looping process. *Aerosol Air Qual. Res.* 17: 2300–2309.

Kuo, Y.L., Huang, W.C., Hsu, W.M., Tseng, Y.H. and Ku, Y. (2015). Use of spinel nickel aluminum ferrite as self-supported oxygen carrier for chemical looping hydrogen generation process. *Aerosol Air Qual. Res.* 15: 2700–2708.

Leion, H., Lyngfelt, A., Johansson, M., Jerndal, E. and Mattisson, T. (2008). The use of ilmenite as an oxygen carrier in chemical-looping combustion. *Chem. Eng. Res. Des*. 86: 1017–1026.

Li, F., Luo, S., Sun, Z., Bao, X. and Fan, L.S. (2011). Role of metal oxide support in redox reactions of iron oxide for chemical looping applications: Experiments and density functional theory calculations. *Energy Environ. Sci.* 4: 3661–3667.

Linderholm, C. and Schmitz, M. (2016). Chemical-looping combustion of solid fuels in a 100 kW dual circulating fluidized bed system using iron ore as oxygen carrier. J. *Environ. Chem. Eng.* 4: 1029–1039.

Liu, Y.C., Ku, Y., Tseng, Y.H., Lee, H.Y. and Kuo, Y.L. (2016). Fabrication of Fe_2O_3/TiO_2 oxygen carriers for chemical looping combustion and hydrogen generation. *Aerosol Air Qual. Res.* 16: 2023–2032.

Luo, M., Wang, S., Wang, L. and Lv, M. (2014a). Reduction kinetics of iron-based oxygen carriers using methane for chemical-looping combustion. *J. Power Sources* 270: 434–440.

Luo, S., Bayham, S., Zeng, L., McGiveron, O., Chung, E., Majumder, A. and Fan, L.S. (2014b). Conversion of metallurgical coke and coal using a coal direct chemical looping (CDCL) moving bed reactor. *Appl. Energy* 118: 300–308.

Luo, S., Zeng, L. and Fan, L.S. (2015). Chemical looping technology: oxygen carrier characteristics. *Annu. Rev. Chem. Biomol. Eng.* 6: 53–75.

Markström, P. and Lyngfelt, A. (2012). Designing and operating a cold-flow model of a 100kW chemical-looping combustor. P*owder Technol.* 222: 182–192.

Markström, P., Linderholm, C. and Lyngfelt, A. (2013). Chemical-looping combustion of solid fuels - design and operation of a 100kW unit with bituminous coal. *Int. J. Greenhouse Gas Control* 15: 150–162.

Mattisson, T., Johansson, M. and Lyngfelt, A. (2004). Multicycle reduction and oxidation of iron oxide particles-application to chemical-looping combustion. *Energy Fuels* 18: 628–637.

Mendiara, T., Abad, A., de Diego, L.F., García-Labiano, F., Gayán, P. and Adánez, J. (2013). Biomass combustion in a CLC system using an iron ore as an oxygen carrier. *Int. J. Greenhouse Gas Control* 19: 322–330.

Mendiara, T., de Diego, L.F., García-Labiano, F., Gayán, P., Abad, A. and Adánez, J. (2014). On the use of a highly reactive iron ore in chemical looping combustion of different coals. *Fuel* 126: 239–249.

Moghtaderi, B. and Song, H. (2010). Reduction properties of physically mixed metallic oxide oxygen carriers in chemical looping combustion. *Energy Fuels* 24: 5359–5368.

Monazam, E.R., Breault, R.W., Siriwardane, R. and Miller, D.D. (2013). Thermogravimetric analysis of modified hematite by methane (CH_4) for chemical-looping combustion: A global kinetics mechanism. *Ind. Eng. Chem. Res.* 52: 14808–14816.

Qin, W., Wang, Y., Dong, C., Zhang, J., Chen, Q. and Yang, Y. (2013). The synergetic effect of metal oxide support on Fe_2O_3 for chemical looping combustion: a theoretical study. *Appl. Surf. Sci.* 282: 718–723.

Shen, L., Wu, J., Xiao, J., Song, Q. and Xiao, R. (2009). Chemical-looping combustion of biomass in a 10 kW_{th} reactor with iron oxide as an oxygen carrier. *Energy Fuels* 23: 2498–2505.

Song, T., Shen, L., Zhang, H., Gu, H., Zhang, S. and Xiao, J. (2012). Chemical Looping Combustion of Two Bituminous Coal/Char with Natural Hematite as Oxygen Carrier in 1 kW_{th} Reactor, Proc. 2nd Int. Conf. on Chemical Looping, Darmstadt, Germany.

Sozinho, T., Pelletant, W., Stainton, H., Guillou, F. and Gauthier, T. (2012). Main Results of the 10 kW_{th} Pilot Plant Operation, Proc. 2nd Int. Conf. on Chemical Looping, Darmstadt, Germany.

Strandberg, M., Olofsson, I., Pommer, L., Wiklund-Lindström, S., Åberg, K. and Nordin, A. (2015). Effects of temperature and residence time on continuous torrefaction of spruce wood. *Fuel Process. Technol.* 134: 387–398.

Ströhle, J., Orth, M. and Epple, B. (2015). Chemical looping combustion of hard coal in a 1 MW_{th} pilot plant using ilmenite as oxygen carrier. *Appl. Energy* 157: 288–294.

Sun, Z., Lu, D.Y., Ridha, F.N., Hughes, R.W. and Filippou, D. (2017). Enhanced performance of ilmenite modified by CeO_2, ZrO_2, NiO, and Mn_2O_3 as oxygen carriers in chemical looping combustion. *Appl. Energy* 195: 303–315.

Thon, A., Kramp, M., Hartge, E.U., Heinrich, S. and Werther, J. (2014). Operational experience with a system of coupled fluidized beds for chemical looping combustion of solid fuels using ilmenite as oxygen carrier. *Appl. Energy* 118: 309–317.

U.S. Energy Information Administration (EIA) (2017). Monthly energy review: August 2017, EIA, U.S. Department of Energy, Washington, DC, USA.

Wang, W., Zhang, B., Wang, G. and Li, Y. (2016). O_2 release of Mn-based oxygen carrier for chemical looping

air separation (CLAS): An insight into kinetic studies. *Aerosol Air Qual. Res.* 16: 453–463.

World Energy Council (WEC) (2016). World Energy Resources 2016, World Energy Council, London, UK.

Wu, H.C., Ku, Y., Tsai, H.H., Kuo, Y.L. and Tseng, Y.H. (2015). Rice husk as solid fuel for chemical looping combustion in an annular dual-tube moving bed reactor. *Chem. Eng. J.* 280: 82–89.

Wu, H.C. and Ku, Y. (2016). Chemical looping gasification of charcoal with iron-based oxygen carriers in an annular dual-tube moving bed reactor. *Aerosol Air Qual. Res.* 16: 1093–1103.

Zafar, Q., Mattisson, T. and Gevert, B. (2006). Redox investigation of some oxides of transition-state metals Ni, Cu, Fe, and supported on SiO_2 and $MgAl_2O_4$. *Energy Fuels* 20: 33–44.

Zhou, Z., Han, L. and Bollas, G.M. (2014). Overview of chemical-looping reduction in fixed bed and fluidized bed reactors focused on oxygen carrier utilization and reactor efficiency. *Aerosol Air Qual. Res.* 14: 559–571.

Zhu, W., Winterstein, J., Maimon, I., Yin, Q., Yuan, L., Kolmogorov, A.N., Sharma, R. and Zhou, G. (2016). Atomic structural evolution during the reduction of α-Fe_2O_3 nanowires. *J. Phys. Chem. C* 120: 14854–14862.

Received for review, August 18, 2018
Revised, April 28, 2019
Accepted, June 19, 2019